Numerical investigation of particle dynamic behaviours in geophysical flows considering solid-fluid interaction

Jun Fang[1], *Yifei* Cui[1*], *Xinyue* Li[2], and *Hui* Tang[3]

[1]State Key Laboratory of Hydroscience and Engineering, Tsinghua University, China
[2]Department of Geotechnical Engineering, College of Civil Engineering, Tongji University, Shanghai, China
[3]Section 4.7: Earth Surface Process Modelling, German Research Centre for Geosciences (GFZ), Potsdam 14473, Germany

Abstract. Solid-fluid interaction vitally influences the flow dynamics of particles in a geophysical flow. A coupled computational fluid dynamics and discrete element method (CFD-DEM) is used in this study to model multiphase geophysical flow as a mixture of fluid and solid phases. The two non-Newtonian fluids (i.e., Bingham and Hershcel-Bulkley fluids) and water mixed with particles are considered in the simulation, while dry granular flow with the same volume is simulated as a control test. Results revealed that the solid-fluid interaction heavily governs the particle dynamic behaviours. Specifically, compared to dry case, particles in three multiphase cases are characterized by larger flow mobility and greater shear rate while smaller basal normal force. In addition, a power-law distribution with a crossover to a generalized Pareto Distribution is recommended to fit the distribution of normalized interparticle contact force.

1 Introduction

Geophysical flows contain a wide type of debris flows, rock avalanches, and snow avalanches based on the classification proposed by Hungr et al. [1]. They can behave like a fluid and move far away from their initial positions with high velocities. Over the past few decades, there have been considerable numerical and experimental investigations to reveal key mechanisms in geophysical flows during their transportation stage, including size segregation, particle breakage and entrainment. Most of these studies have considered geophysical flows into either pure fluids or dry particles, with only a small amount in water-particle mixtures [2-5]. However, it is well known that the solid and fluid phases vitally influence geophysical flow dynamics [6], and gross simplification will inhibit a comprehensive understanding of two-phase interaction.

In this study, the focus is placed on the effect of solid-fluid interaction on particle mechanical behaviour in a mixture composed of granular and fluids, where a Newtonian (water) and two non-Newtonian fluids (Bingham and Herschel-Bulkley fluids) are adopted to model the liquid phase, corresponding to Case W-P, Case B-P, Case HB-P, respectively. In reality, fluids in geophysical flows, such as slurry, are commonly complicated in terms of rheological properties and exhibit non-Newtonian behaviour. Considering non-Newtonian fluids provide better explorations of more complex natural flows than Newtonian fluids like water only. In addition, the dry granular flow (Case P) with the same volume is simulated as a control test.

2 Methodology and model setup

2.1 Methodology

The solid particles are regarded as a discrete phase that is modelled by the discrete element method (DEM), while the fluid is a continuous system simulated by the computational fluid dynamics method (CFD). It is assumed that the translational and rotational motions of each particle are controlled by Newton's equations of motion, and the continuous fluid system can be described by locally averaged Navier-stokes equation. The key to the coupling between the CFD and DEM is to properly consider the particle-fluid interaction forces, including drag force and buoyancy force. More details about CFD-DEM can be found in the literature [5, 7].

2.2 Model setup

Fig. 1 shows the schematic of the CFD-DEM model simulating fluid and particle mixture flow collapse onto an inclined channel. A gravity-driven mixture sample (H = 0.3 m, L = 0.5 m, W = 0.3 m) composed of viscous fluid and particles is first produced in a pre-defined area before being released to flow along the flume base to impact the rigid barrier. Note that for dry granular flow, only particles are generated in the pre-defined area. After the packing is stable, the flume will be rotated by 20°. Then the door will be removed, and the particles will flow along the flume base. In the initial state, for mixture flows, it is assumed that only the fluid cells in

* Corresponding author: yifeicui@mail.tsinghua.edu.cn

the initial deposition domain contain water while the rest of the CFD fluid cells is air. The DEM time step is adopted based on the criteria of the Rayleigh time[8], whilst the CFD time step is determined as 100 times larger than that of the DEM to ensure sufficient accuracy and efficiency.

As summarized in Table 1, besides water, there are two non-Newtonian fluids (Bingham and Herschel-Bulkely fluids) adopted to simulate the complex fluid in geophysical flow. The particle parameters have also been listed in Table 1. Interested readers can find the details of benchmarks of particle and fluid properties in literature (e.g., Li and Zhao [9], Fang et al. [5]).

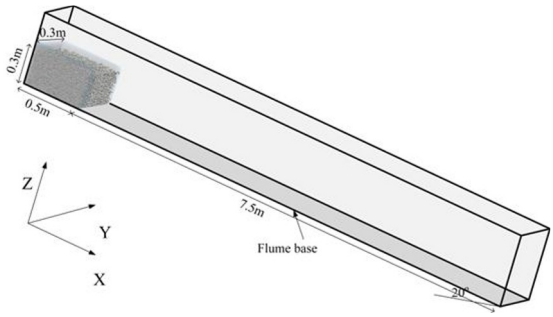

Fig. 1. Model setup for CFD-DEM simulation

Table 1. Input parameters adopted for the CFD-DEM model

Material type	Parameters	Values
Particle	Barrier Young's modulus (Pa)	3.2×10^{9}
	Particle Young's modulus (Pa)	6×10^{10}
	Coefficient of restitution	0.78
	Particle density (Kg/m³)	2550
	Gravitational acceleration (m/s²)	9.81
	Inter-element friction coefficient	0.48
	Interface-element friction coefficient	0.4
	Particle diameter (mm)	10
	Particle Poisson ratio	0.25
	Barrier Poisson ratio	0.35
Air	Viscosity (Pa·s)	1.48×10^{-5}
	Density (Kg/m³)	1.0
Water	Viscosity (Pa·s)	1×10^{-3}
	Density (Kg/m³)	1000
Bingham fluid	Density ρ (Kg/m³)	1400
	Consistency index k (Pa·sⁿ)	4
	Flow index n	1
	Yield stress τ_0 (Pa)	2.1
Herschel-Bulkley fluid	Density ρ (Kg/m³)	1000
	Consistency index k (Pa·sⁿ)	4.279
	Flow index n	0.479
	Yield stress τ_0 (Pa)	30.002
Simulation control	DEM time step (s)	5×10^{-7}
	CFD time step (s)	5×10^{-5}
	Simulated time interval	100

3 Results

3.1 Flow regimes

Fig. 2a shows the computed flow dynamics of dry granular flow (Case P) at three typical instants. It can be seen that, after releasing, the right portion of the particle column is mobilized by gravity with a wedge front, while the left still remains static. During the flow process, the depositing height reduces, and moving particles become dominant. For comparison, the flow evolutions of the water and particle mixture flow (Case W-P) are presented in Fig. 2b. Unlike dry granular flow, water and particle mixture flow exhibits a larger spreading velocity, and a longer flow distance can be observed simultaneously. In addition, due to solid-fluid interaction, the collisions between particles are weakened, and the phenomenon where dispersed particles move ahead of the flow front and detach from subsequent particles is not obvious in Case W-P.

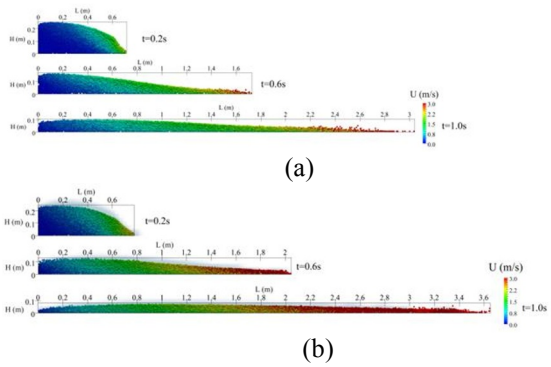

Fig. 2. Flow process for Case P (a) and Case W-P (b)

It is apparent the solid-fluid interaction can influence the flow dynamics. We further analyze the vertical centre of particle position z, as shown in Fig. 3. The vertical centres of particle position of three mixture cases are lower than that of Case P, which signifies that the particles in the three mixture cases collapse faster. This is caused by the solid-fluid interaction, where the fluid can impose a driving force to enhance the flow dynamics of the particles and a buoyant force to reduce the interparticle collision [10]. Furthermore, it should be noted that there are also some differences among the three mixture flows, where vertical centres of particle position in Case B-P slightly deviate from the other two mixture flow (Case W-P and Case HB-P). The higher density of Bingham fluid may explain this phenomenon compared to the other two fluids in the mixture cases, which can provide greater dragging and buoyancy force on the particles [9].

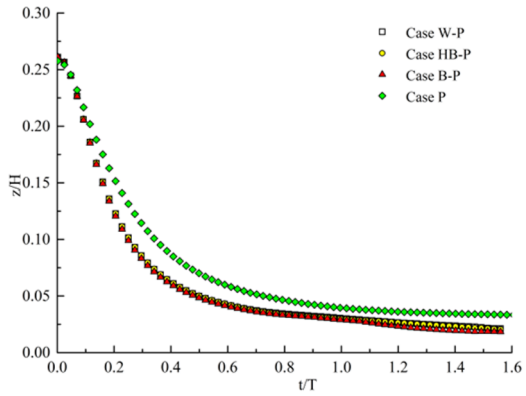

Fig. 3. Time evolution of the vertical centre of particle position z, where $\mathbf{z} = \frac{1}{n}\sum_{i=1}^{n} \boldsymbol{z_i}$, where n and z_i denotes particle number and vertical centre height of i^{th} particle, respectively. The normalizer of time is calculated as $\mathbf{T} = \sqrt{\boldsymbol{gH}}$, where $\boldsymbol{H}$ is the flow thickness and $\boldsymbol{g}$ is gravitational acceleration

During the transportation process, shearing is developed along with the flowing thickness and the traveling direction. Fig. 4 shows the computed velocity distribution along the normal and traveling direction for four geophysical flows at t=0.6s, and the corresponding flow profile is also presented. Different symbols are adopted to represent the particle velocities at the different positions along flow thickness, where the distance of particles is scaled away from the rear ($L^* = 0$) to the front ($L^* = 1$). The reciprocal values of the fitted curve slopes represent shear rates. The results show that the shear rate in the particles increases from the rear to the front along the flow direction for all cases. An apparent increase in the shear rate near the bottom is observed, which indicates that there is a boundary layer developing. The boundary effect of the flume base may be responsible for this.

In this study, it can be found the velocity profiles are mainly in power-law distribution:

$$H \sim (v)^k \tag{1}$$

The nature seems to be independent on the properties of the incoming flow. Compared with the three mixture cases, the dry granular flow (Case P) has a smaller k value along the flow direction, which implies a weakened shearing of the granular materials. Especially at the location of $L^* = 0.1$, the fitting curve of Case P shows upper convex with k smaller than 1.0, while the lower convex tendency is observed in other fitting curves with k larger than 1.0. Because of different fluid properties, including density and viscosity, the minor difference can also be found among the three mixture, where Case B-P has a maximum shear rate.

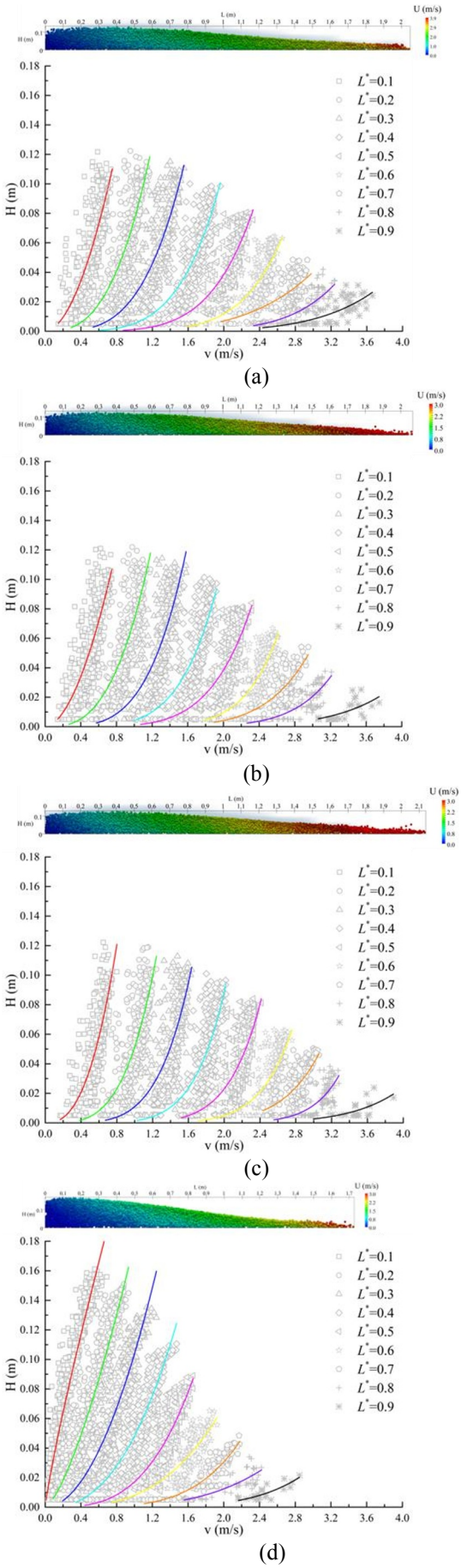

Fig. 4. Computed velocity distribution along the height and traveling direction for four geophysical flows at t = 0.6s: (a) Case W-P; (b) Case HB-P; (c) Case B-P; (d) Case P

3.2 Basal normal force

Basal normal force F_n is caused by the impact of particles, which is composed of single free particle impact F_n^s and multiple particle impact F_n^c. The single free particle impact F_n^s is caused by particles free from surrounding particles. And the multiple particle impact F_n^c results from the impact of particles that also have a collision with other particles with a force chain effect [11]. Fig. 5 shows the development of the basal normal force of four geophysical flows, normalized by the total weight of particles. And the ratio of F_n^s and F_n is also added in the figure.

As shown, at the initial stage, the basal normal force F_n has a small fluctuation, then reaches a static state. After stabilization, the magnitude of F_n of four cases evolves in the following order: Case P > Case W-P > Case HB-P > Case B-P. The differences are mainly attributable to the collective effect of the density and viscosity of the fluid, which further influences the solid-fluid interaction. In addition, it can be found that at the beginning, the basal normal force generated by multiple particle impact F_n^c is the main component, then gradually decreases during the flowing process. The corresponding impact load of a single free particle F_n^s plays a more important role, with F_n^s/F_n approaching 1.0. This phenomenon indicates that more particles tend to be dispersed and free from surrounding particles in the flow evolution. But for dry granular flow (Case P), it would take longer for particles to become dispersed.

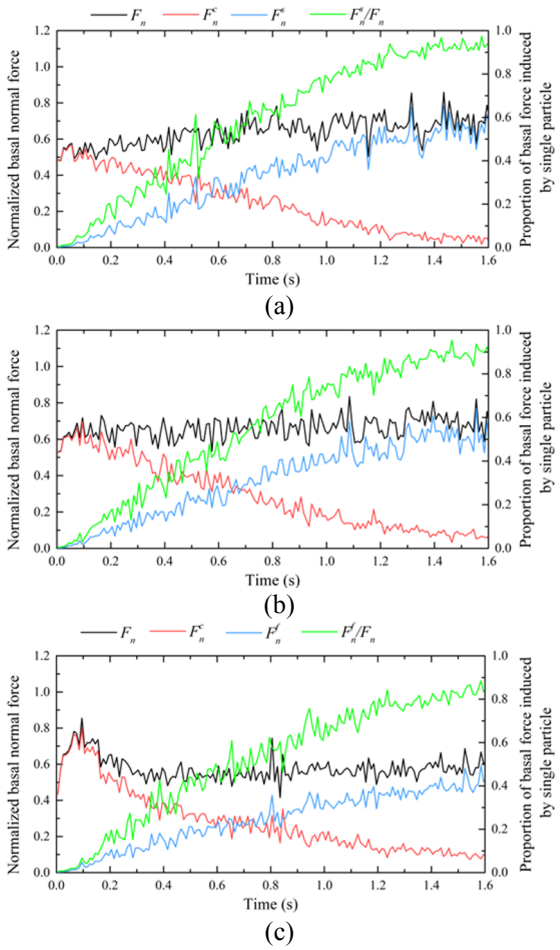

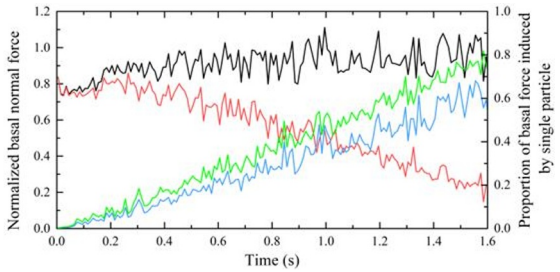

Fig. 5. Computed velocity distribution along the height and traveling direction for four geophysical flows: (a) Case W-P; (b) Case HB-P; (c) Case B-P; (d) Case P

3.3 Interparticle contact force

Fig. 6 shows the semilogarithmic plots of probability density function P(*f*) of the interparticle contact forces *N* in the four cases at three typical moments. The contact force *N* is normalized by the average contact force <*N*>. According to Radjai et al. (1996) [12], the data for forces lower than the mean have a power-law distribution (Power), while the rest data can be well fitted by an exponential decay (Exp). However, except at the initial instants, the force distributions above the mean deviate from this behaviour, which decays more slowly than an exponential. A generalized Pareto Distribution (GPD) is introduced to fit the pdfs of contact forces larger than the mean [13], which shows a better performance than exponential behaviour. We conclude that the distribution of normalized contact forces is independent of our incoming flow properties and can be approximated by a power-law decay with a crossover to a GPD distribution:

$$\begin{cases} P(f) = a * (N/< N >)^b & , N << N > \\ P(f) = \left(\frac{1}{A}\right)\left(1 + B\frac{(N/<N>)-C}{A}\right)^{\left(-1-\frac{1}{B}\right)} & , N >< N > \end{cases} \quad (2)$$

where a, b, A, B and C are constant parameters. The fitting lines have been reported in Fig. 6 and the values of parameters a, b, A, B and C are also indicated.

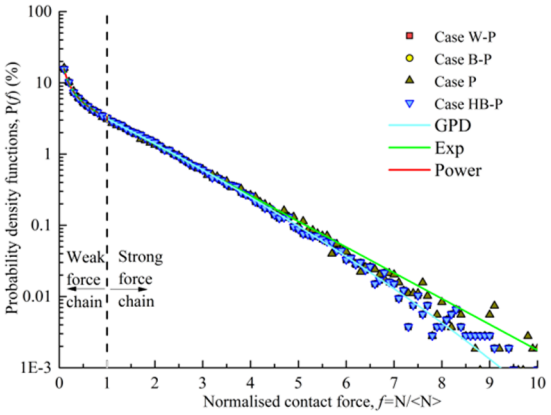

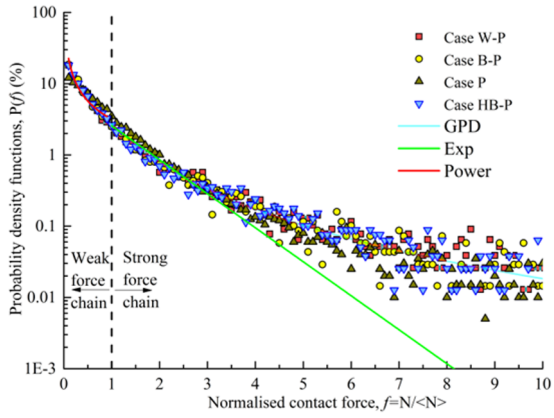

(b)

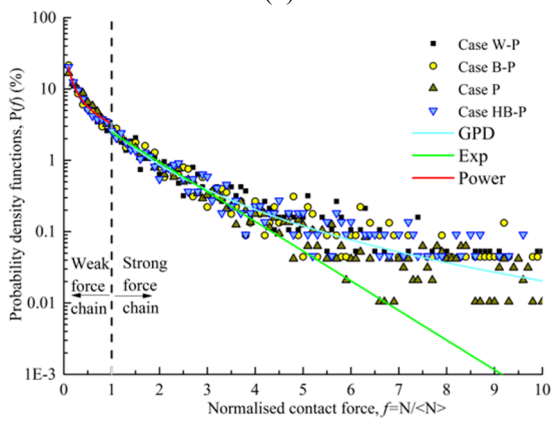

(c)

Fig. 6. Computed probability density functions of inter-particle normalised contact force: (a) t=0.0s, a=3.31, b=-0.67, A=1.12, B=-0.05, C=2.53; (b) t=0.6s, a=3.17, b=-0.85, A=1.76, B=0.57, C=2.35; (c) t=1.0s, a=3.27, b=-0.79, A=1.90, B=0.50, C=2.58

4 Conclusions

The effect of solid-fluid interaction on particle behaviours in geophysical flows has been examined using a coupled CFD-DEM model. It was found that the solid-fluid interaction has a remarkable influence on the flow mobility and flow regimes of particles in geophysical flows. Compared with the dry granular flow, particles in three mixture cases have a larger flow dynamic and an enhanced shear rate along flow direction and flow thickness. In addition, the geophysical fluid can accelerate the dispersion of particles, and the impact of single dispersed particles would become the main source of basal normal force. A combination of power-law decay and GPD is suggested to fit the probability density function of the normalized interparticle contact force for four cases.

This study is funded by the National Natural Science Foundation of China (42120104002, 41941019), the Second Tibetan Plateau Scientific Expedition and Research Program (2019QZKK0903), and the Research Fund Program of the State Key Laboratory of Hydroscience and Engineering (2021-KY-04).

References

1. O. Hungr, S. Leroueil, L Picarelli, Landslides **11(2)**, 167–194 (2014)
2. N. Balmforth, R. Kerswell, J. Fluid Mech. **538**, 399–428 (2005)
3. Z. Lai, L. E. Vallejo, W. Zhou, G. Ma, J. M. Espitia, B. Caicedo, X. Chang, Geophys. Res. Lett., **44(24)**, 12–181 (2017)
4. A. Leonardi, G. R. Goodwin, M. Pirulli, Acta Geotech. **14(6)**, 1949–1963 (2019)
5. J. Fang, L. Z. Wang, Y. Hong, J. D. Zhao, Géotechnique **72(5)**, 1–62 (2022)
6. R. M. Iverson, Reviews of Geophysics **35(3)**, 245-296 (1997)
7. J. Zhao, T. Shan, Powder Technol., **239(17)**, 248-258 (2013)
8. E. M. Smuts, D. A. Deglon, C. J. Meyer, *Methodology for CFD-DEM modelling of particulate suspension rheology*, in Proceedings of the Ninth International Conference on CFD in the Minerals and Process Industries CSIRO, Melbourne, Australia, 37–53 (2012).
9. X. Li, J. Zhao, Powder Technol. **338**, 493–505 (2018)
10. J. Fang, Y. F. Cui, X. Y. Li, J. Y. Nie,. Computers and Geotechnics **148**, 104790, (2022)
11. J. Estep, J. Dufek. Journal of Geophysical Research **117**, F01028 (2012)
12. F. Radjai, M. Jean, J.-J. Moreau, S. Roux, Phys. Rev. Lett. **77 (2)**, 274–277 (1996)
13. S.W. McCoy, G. Tucker, J. Kean, J. Coe. J. Geophys. Res. Earth Surf. **118 (2)**, 589–602 (2013).